Electronic Supplementary Material (ESI) for Dalton Transactions.

A stable mixed lanthanide metal-organic framework for highly sensitive thermometry

Yue Pan,[a] Hai-Quan Su,*[a] En-Long Zhou,*[b] Hong-Zong Yin*[b] Kui-Zhan Shao,[c] Zhong-Min Su*[c]

School of Chemistry and Chemical Engineering, Inner Mongolia University, 235 West Daxue Road, Hohhot 010021, China, E-mail: haiquansu@yahoo.com

College of Chemistry and Material Science, Shandong Agricultural University, Tai'an, 271018, P. R. China. E-mail: iamelzhou@njtech.edu.cn

Institute of Functional Material Chemistry, National & Local United Engineering Lab for Power Battery, Northeast Normal University, Changchun, 130024 Jilin, P. R. China. E-mail: zmsu@nenu.edu.cn

Materials and Instrumentation:

All chemicals were obtained commercially and used without any additional purification. Single-crystal diffractometry was conducted on a Bruker Smart Apex CCD II area-detector diffractometer with graphite-monochromated Mo Kα radiation (λ = 0.71073 Å) at room temperature. Elemental analyses (C, H, and N) were performed on a Perkin-Elmer 2400 CHN elemental analyzer and the metal contents were determined with a PLASMA-SPEC(I) ICP atomic emission spectrometer. IR spectra were recorded in the range 4000-400 cm^{-1} on Mattson Alpha-Centauri spectrometer using KBr pellets. Thermal gravimetric (TG) analyses were performed on a Perkin-Elmer TGA7 instrument in flowing N_2 with a heating rate of 10 °C/min. Powder X-ray diffraction (XRD) measurements were performed on a Rigaku D/MAX-3 instrument with Cu Kα radiation in the angular range 2θ = 3°-50° at 293 K. Temperature-dependent X-ray diffraction experiments were performed on an Ultima-IV X-ray diffractometer with a step size of 0.02° in 2θ. Emission and excitation spectra in the solid state were investigated on the F-4500 FL spectrophotometer. The temperature dependence of luminescence (77-377 K range) was investigated by setting the sample in a cryostat (OptistatDN2, Oxford Instruments). Temperature-dependent decay curves were recorded on a Horiba Delta Flex equipped with different excitation sources.

Synthesis of compound 1 to 3

A mixture of $Eu(NO_3)_3 \cdot 6H_2O$ (46 mg, 0.1 mmol) and H_4BPTC (17 mg, 0.05 mmol) were mixed in solvent of N, N-dimethylformamide (DMF, 6 mL) and distilled water (2 mL). The mixtures were stirred for 15 minutes and were transferred to a Teflon-lined stainless steel vessel (15 mL) and heated to 100 °C. After maintaining at this temperature for two days, the Teflon-lined stainless steel vessel cooled to room temperature naturally. The resulting colorless rodlike crystals of **1** were obtained and washed by distilled water and DMF, yielding 78% based on Eu^{3+}. Calcd (%) for $C_{18}H_{14}NO_8Eu$ (524.27): C 41.24, H 2.69, N 2.67; found: C 41.19, H 2.74, N 2.58. Compound **2** was obtained in 87% yield in a way similar to that described for **1** by using $Tb(NO_3)_3 \cdot 6H_2O$ instead of $Eu(NO_3)_3 \cdot 6H_2O$. Calcd (%) for $C_{18}H_{14}NO_8Tb$ (531.23): C 40.70, H 2.66, N 2.64; found: C 40.78, H 2.54, N 2.57.

The same procedure was used for the synthesis of mixed compound **3** by using a mixture of $Eu(NO_3)_3 \cdot 6H_2O$ and $Tb(NO_3)_3 \cdot 6H_2O$ as metal sources.

X-ray Crystallography:

Single-crystal diffractometry was conducted on a Bruker Smart Apex CCD II area-detector diffractometer with graphite-monochromated Mo K_α radiation (λ = 0.71073 Å) at room temperature. The linear absorption coefficients, scattering factors for the atoms, and anomalous dispersion corrections were taken from the International Tables for X-Ray Crystallography. Empirical absorption corrections were applied. The structures were solved by using the direct method and refined through the full-matrix least-squares method on F2 using SHELXS-97.

Crystal data of **1**: Trigonal, Fw = 478.17 g/mol, space group $P3_1$, Z = 6, a = 13.8165 (16) Å, b = 13.8165 (16) Å, c = 22.984 (3) Å, $\alpha = \beta = 90$ deg, $\gamma = 120$ deg, V = 3799.7(12) $Å^3$, T = 296 (2) K, 23781 reflections measured, 5021 independent reflections (R_{int} =

0.0389). The final R_1 values were 0.0277 (I> 2σ(I)). The final $wR(F^2)$ values were 0.0598 (I> 2σ(I)). The goodness of fit on F^2 was 0.927.
Crystal data of **2**: Trigonal, Fw = 485.14 g/mol, space group $P3_1$, Z = 6, a = 13.825 (5) Å, b = 13.825 (5) Å, c = 22.984 (5) Å, $\alpha = \beta$ = 90 deg, γ = 120 deg, V = 3804(3) Å^3, T = 296 (2) K, 26250 reflections measured, 5626 independent reflections (R_{int} = 0.0451). The final R_1 values were 0.0293 (I> 2σ(I)). The final $wR(F^2)$ values were 0.0593 (I> 2σ(I)). The goodness of fit on F^2 was 0.946.

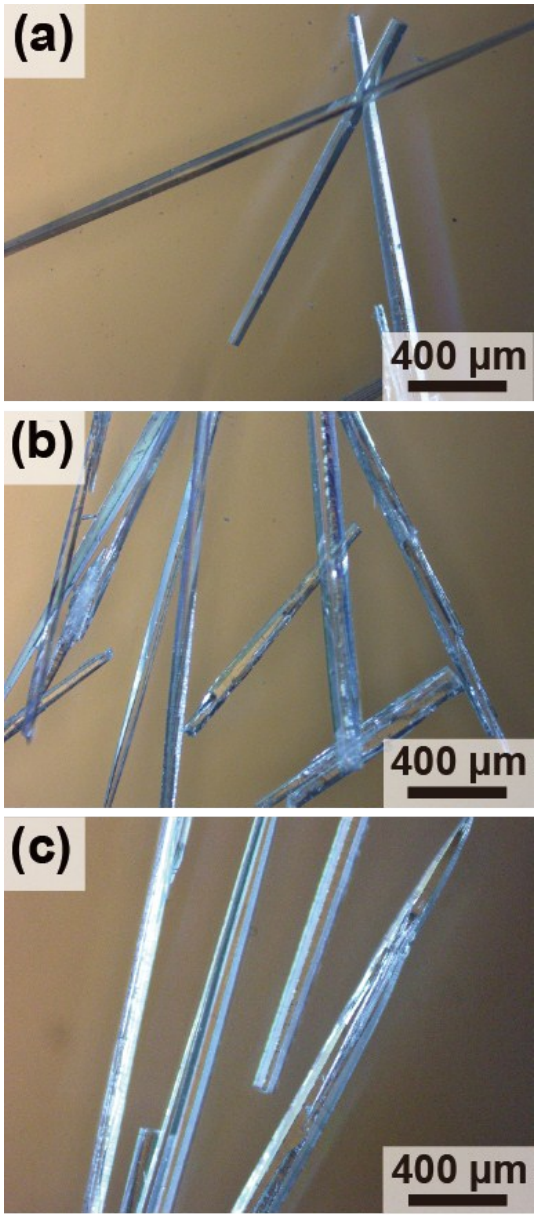

Figure S1. Optical micrographs of (a) compound **1**, (b) compound **2** and (c) compound **3**.

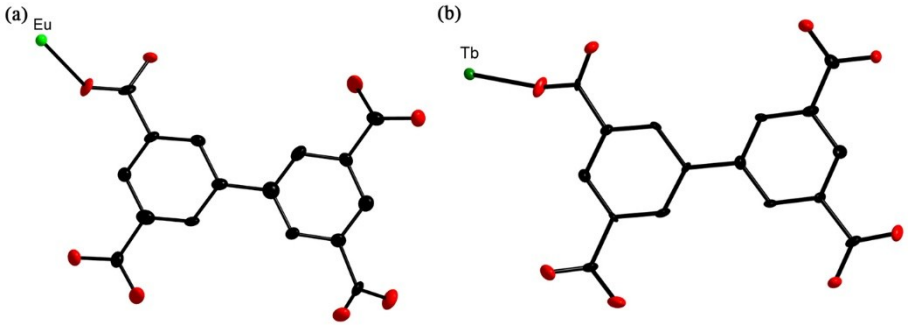

Figure S2. The ORTEP-style image of the asymmetric unit of (a) compound **1** and (b) compound **2.**

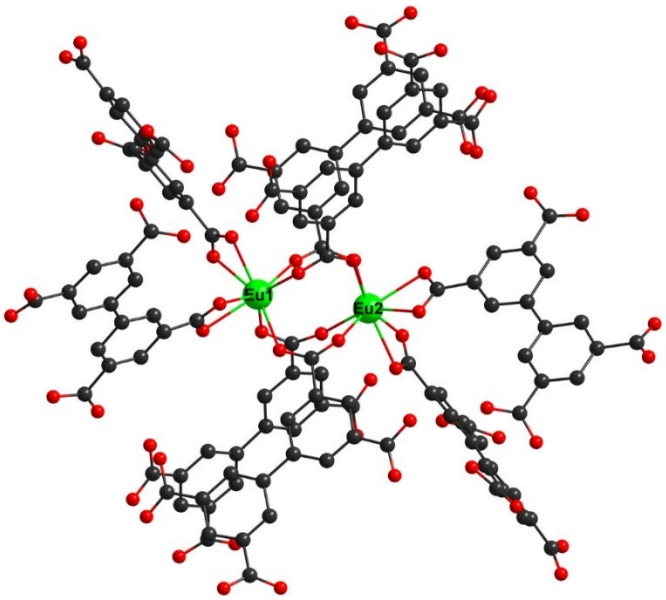

Figure S3. The coordination environment of Eu^{3+} in compound **1.**

Table S1. Selected Eu-O bond lengths (Å) of compound **1**

Compound **1**			
Eu1-O1	2.309	Eu2-O2	2.389
Eu1-O5	2.389	Eu2-O3	2.480
Eu1-O7	2.439	Eu2-O4	2.481
Eu1-O8	2.521	Eu2-O6	2.319
Eu1-O10	2.392	Eu2-O9	2.328
Eu1-O11	2.462	Eu2-O13	2.378
Eu1-O12	2.484	Eu2-O15	2.553
Eu1-O14	2.331	Eu2-O16	2.467

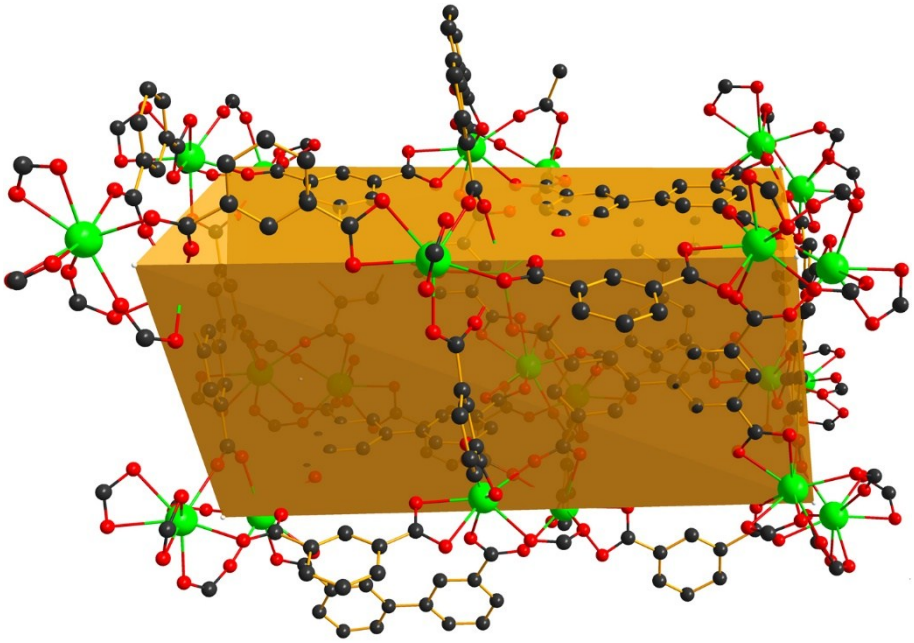

Figure S4. The parallelogram cage constructed by 24 nuclear Eu^{3+} ions.

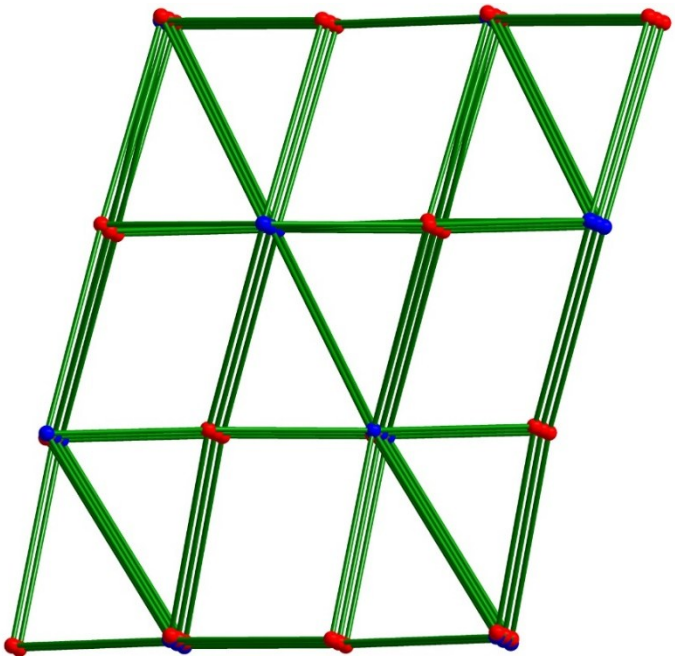

Figure S5. The topology of compound **1** viewed along *b* axis.

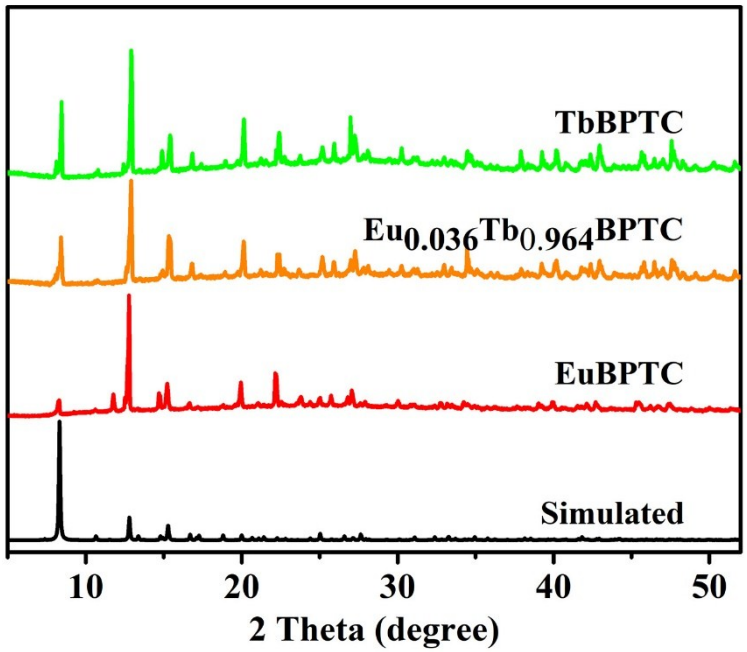

Figure S6. Comparision of powder X-ray diffraction patterns of EuBPTC, TbBPTC, and their mixed sample with that simulated from the X-ray single structure.

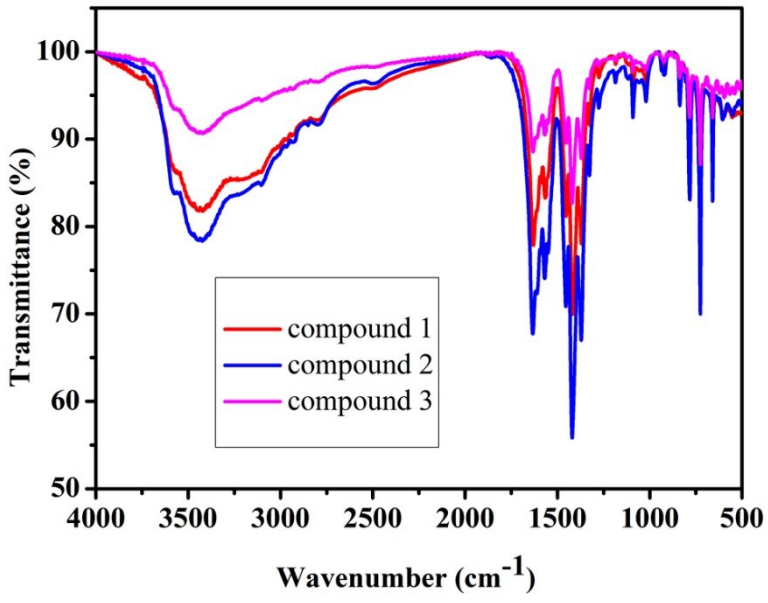

Figure S7. The IR spectroscopy of compound **1**, compound **2** and compound **3**.

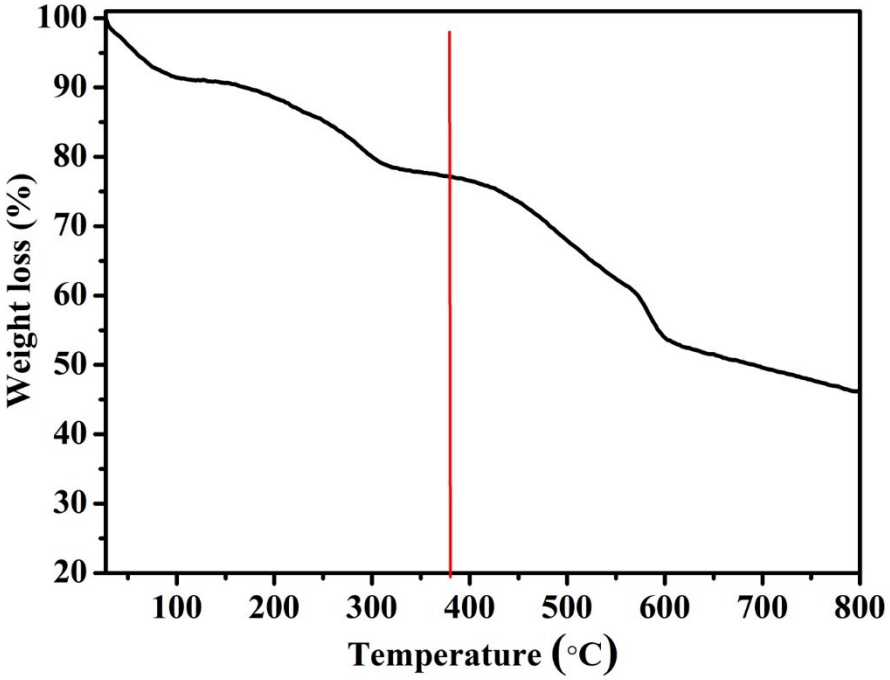

Figure S8. The TG curve of compound **1**.

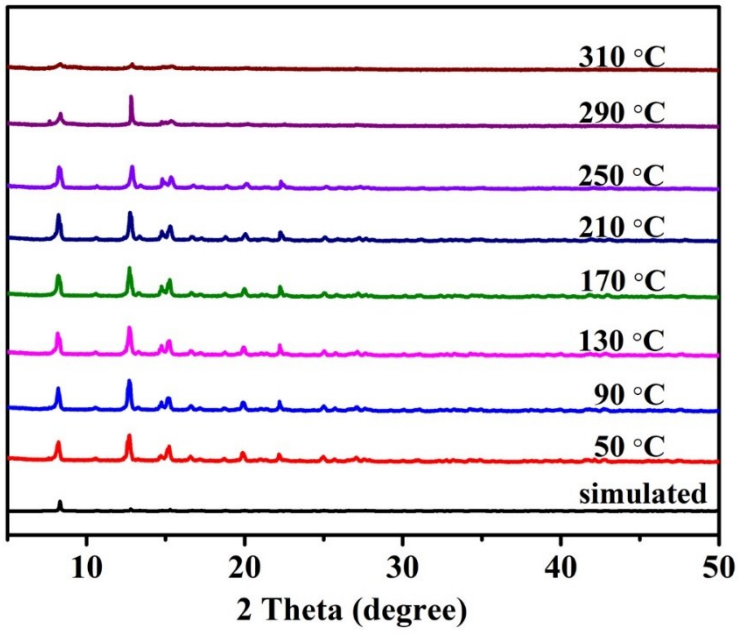

Figure S9. *In situ* variable-temperature powder X-ray diffraction of compound **1**.

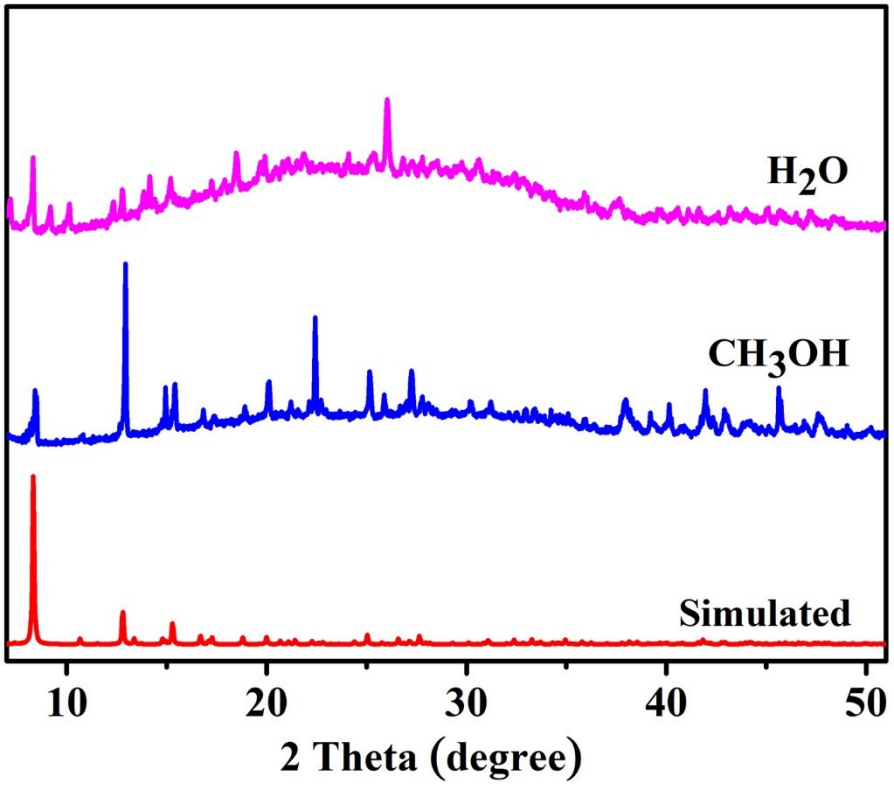

Figure S10. Powder X-ray diffraction of compound **1** after immersed in different solvents at 100 ℃ for 3 days.

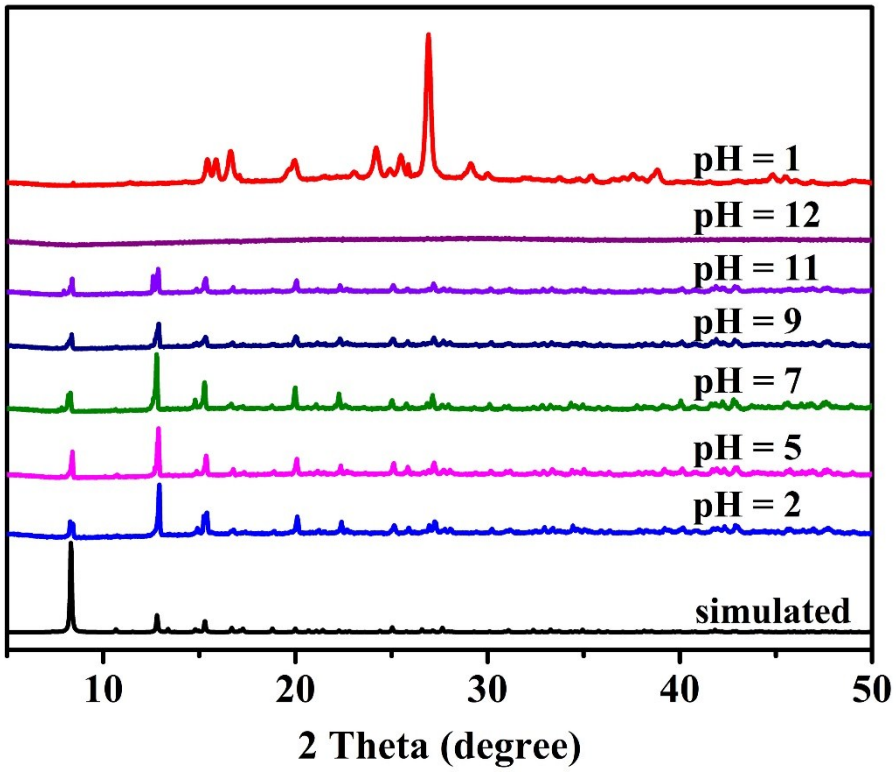

Figure S11. Powder X-ray diffraction of compound **1** after immersed in different pH solution for 24 h.

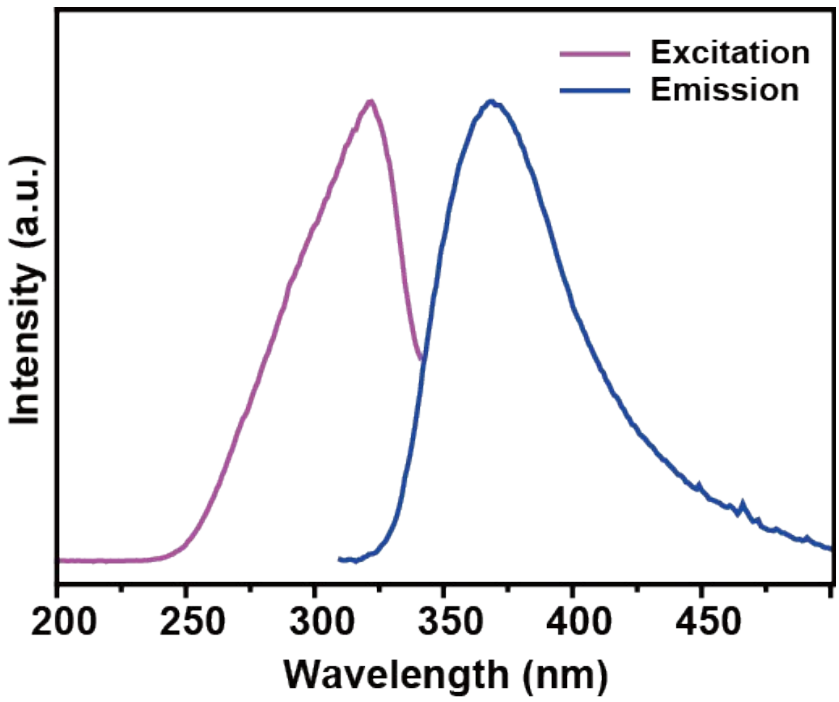

Figure S12. Excitation and emission spectra of the H_4BPTC ligand.

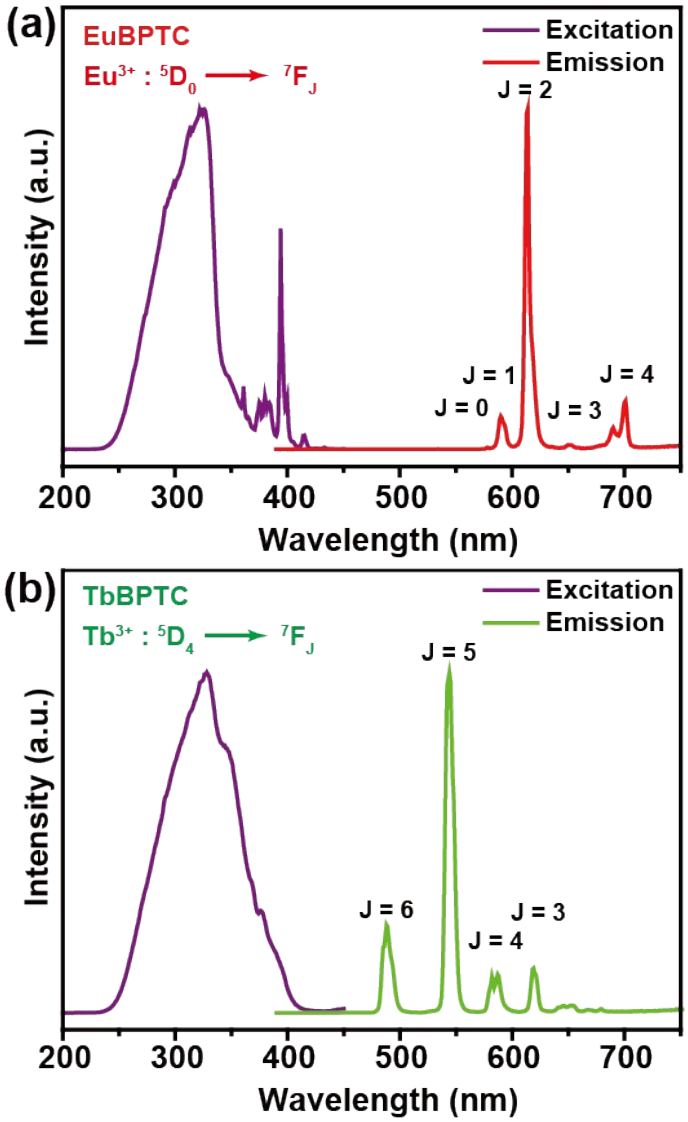

Figure S13. Excitation and emission spectra of the compound **1** (a) and compound **2** (b).

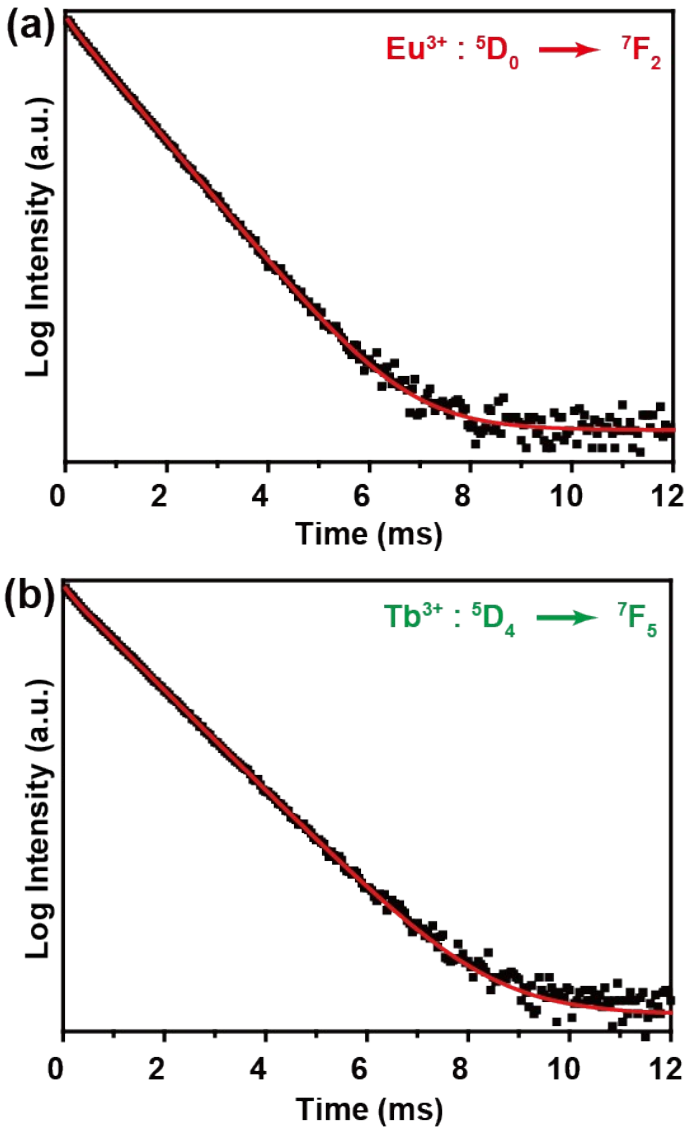

Figure S14. The decay curves of the compound **1** (a) monitored at 614 nm and compound **2** (b) monitored at 544 nm.

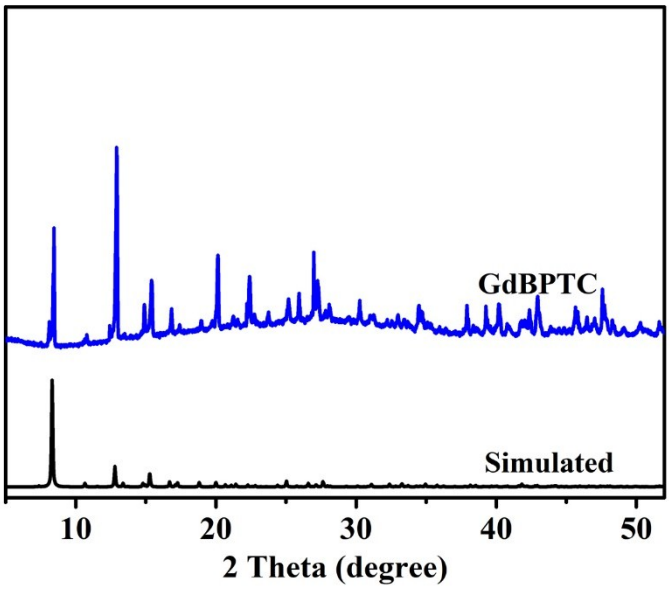

Figure S15. PXRD patters of GdBPTC and that simulated from EuBPTC.

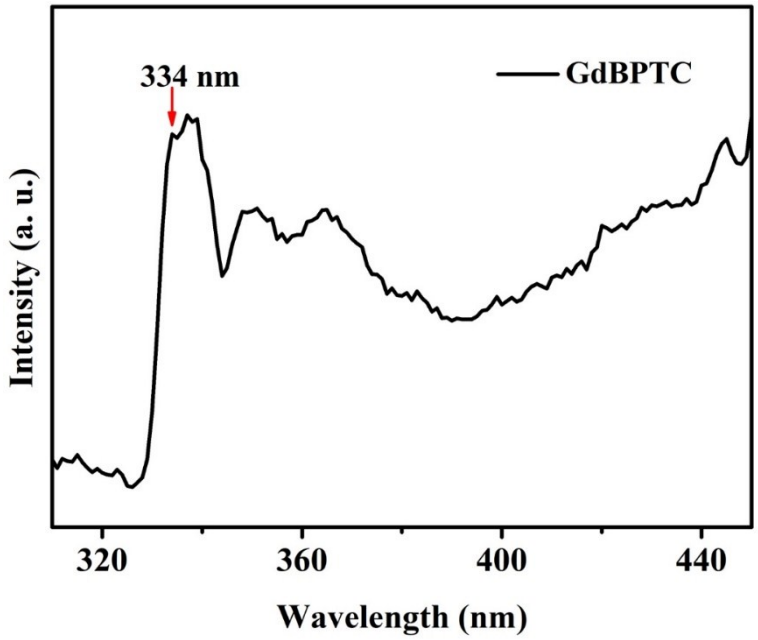

Figure S16. Emission spectrum of GdBPTC at 77 K.

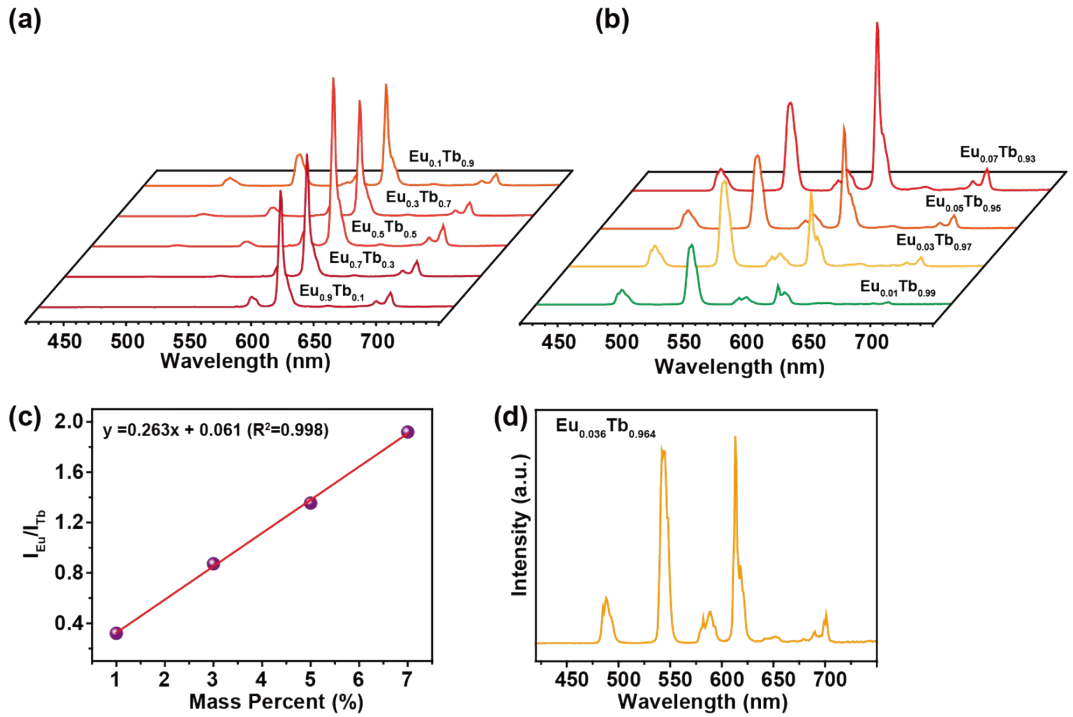

Figure S17. (a) (b) Emission spectra of different Eu^{3+}/Tb^{3+} molar in MOFs. (c)Relation between I_{Eu}/I_{Tb} and Eu content in MOFs. (d) Emission spectra of $[(CH_3)_2NH_2]Eu_{0.036}Tb_{0.964}BPTC$ at room temperature.

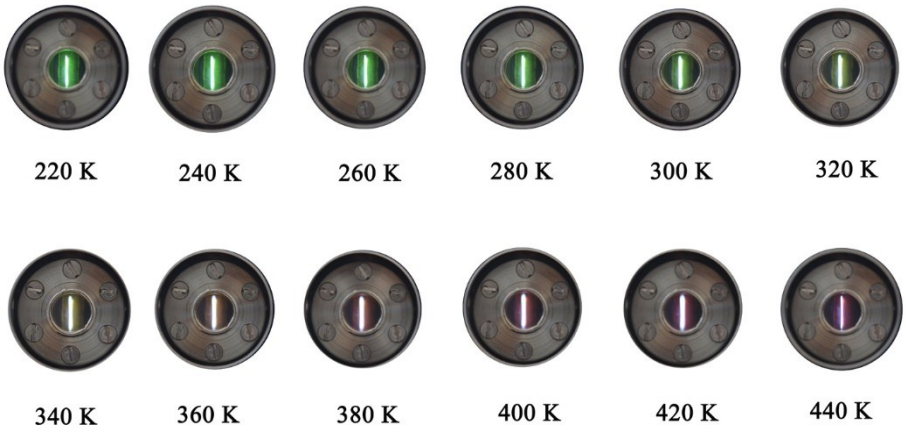

Figure S18. Temperature-dependent photographs of mixed Ln-MOF under UV excitation.

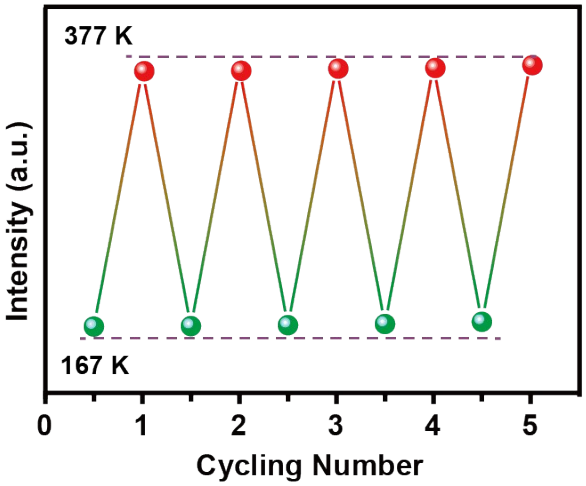

Figure S19. Reversible changes of emission intensity ratio of Eu^{3+} (545 nm) to Tb^{3+} (614 nm) of compound 3 by temperature cycling between 167 K and 377 K.

Table S2 Overview of the relative sensitivity S_r for chosen recently reported Eu,Tb co-doped MOFs.

Materials	Temp. range (K)	Max. S_r (% K^{-1})	Ref.
$Tb_{0.95}Eu_{0.05}$(btb)	10-320	2.85	1
$Eu_{0.0069}Tb_{0.9931}$DMBDC	50-200	1.15	2
$Tb_{0.9}Eu_{0.1}$PIA	100-300	3.27	3
$Eu_{0.19}Tb_{0.81}$PDDI	313-473	0.37	4
$[Eu_{0.7}Tb_{0.3}$(D-cam)$(Himdc)_2(H_2O)_2]_3$	100-450	0.11	5
$Eu_{0.37}Tb_{0.63}$-BTC-a	313-473	0.17	6
Eu@UIO-66-Hybrid film	303-403	2.11	7
$Tb_{0.99}Eu_{0.01}(BDC)_{1.5}(H_2O)_2$	290-320	0.31	8
$Tb_{0.957}Eu_{0.043}$cpda	40-300	16	9
$(Tb_{0.914}Eu_{0.086})_2(PDA)_3(H_2O)]\cdot 2H_2O$	10-325	5.96	10
ZJU-88⊃perylene	293-353	1.28	11
Eu,TbPOM@MOF	60–360	0.71	12
$Tb_{0.80}Eu_{0.20}$(bpda)	303–328	1.39	13

$[Tb_{0.99}Eu_{0.01}(hfa)_3(dpbp)]n$	200–300	0.52	14
$[(CH_3)_2NH_2]Eu_{0.036}Tb_{0.964}BPTC$	220-310	9.42	This work

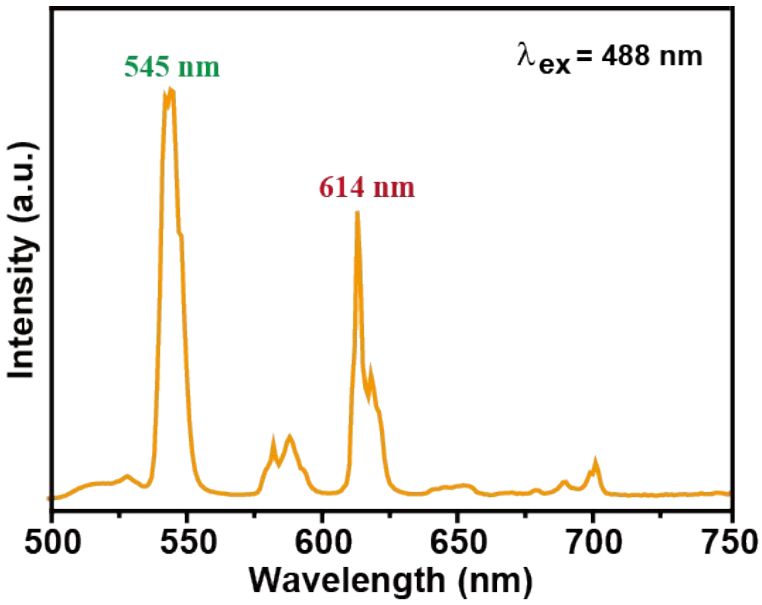

Figure S20. Room temperature emission spectra of $[(CH_3)_2NH_2]Eu_{0.036}Tb_{0.964}BPTC$ excited at 488 nm.

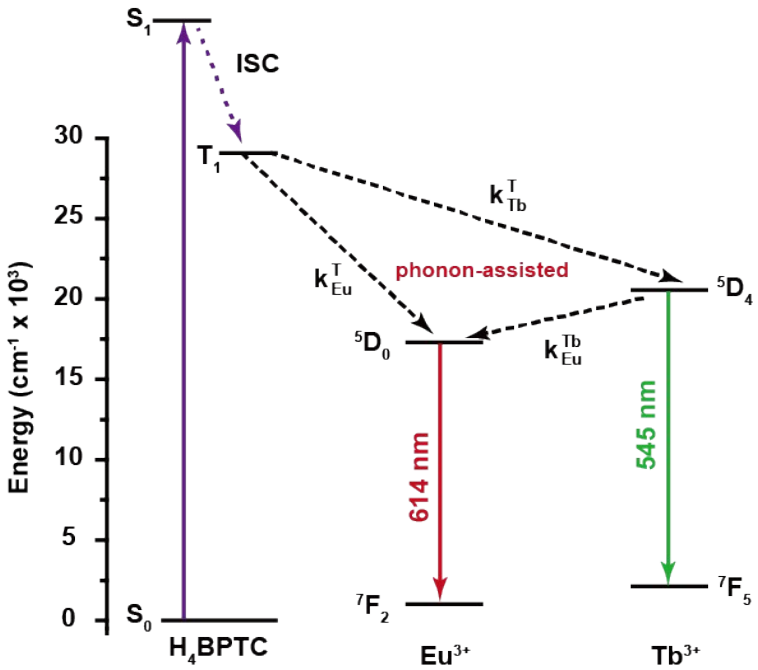

Figure S21. Schematic illustration of luminescence generation in MOFs. Abbreviations: S = singlet; T = triplet; ISC = intersystem crossing; k = nonradiative and radiative transition probability. The solid arrows represent absorption and radiative transitions; dotted arrows indicate nonradiative transitions.

1. D. Ananias, C. D. S. Brites, L. D. Carlos, J. Rocha, Eur. J. Inorg. Chem., 2016, 1967.
2. Y. J. Ciu, H. Xu, Y. F. Yue, Z. Y. Guo, J. C. Yu, Z. X. Chen, J. K. Gao, Y. Yang, G. D. Qian and B. L. Chen, J. Am. Chem. Soc., 2012, 134, 3979.
3. X. Rao, T. Song, J. Gao, Y. Cui, Y. Yang, C. Wu, B. Chen and G. Qian, J. Am. Chem. Soc., 2013, 135, 15559.
4. D. Zhao, H. Wang, G.Qian, CrystEngComm, 2018, 20,7395.
5. Y. H. Han, C. B. Tian, Q. H. Li and S. W. Du, J. Mater. Chem. C, 2014, 2, 8065.
6. H. Wang, D. Zhao, Y. Cui, Y. Yang and G. Qian, J. Solid State Chem., 2017, 246, 341.
7. J. Feng, S. Gao, T. Liu, J. Shi, and R. Cao, ACS Appl. Mater. Interfaces, 2018, 10, 6014.
8. A. Cadiau, C. D. S. Brites, P. M. F. J. Costa, R. A. S. Ferreira, J. Rocha and L. D. Carlos, ACS Nano, 2013, 7, 7213.
9. Y. J. Cui, W. F. Zou, R. J. Song, J. C. Yu, W. Q. Zhang, Y. Yang and G. D. Qian, Chem. Commun., 2014, 50, 719.
10. Z. Wang, D. Ananias, A. Carne-Sanchez, C. D. S. Brites, I. Imaz, D. Maspoch, J. Rocha and L. D. Carlos, Adv. Funct. Mater., 2015, 25, 2824.
11. Y. J. Cui, R. J. Song, J. C. Yu , M. Liu., Z. Q. Wang, C. D. Wu, Y. Yang, Z. Y Wang, B. L. Chen and G. D. Qian, *Adv. Mater.*, 2015, 27, 1420.
12. A. M.Kaczmarek, J. Mater. Chem. C, 2018, 6, 5916.
13. D. Zhao, X. Rao, J. Yu, Y. Cui, Y. Yang and G. Qian, Inorg. Chem., 2015, 54, 11193.
14. K. Miyata, Y. Konno, T. Nakanishi, A. Kobayashi, M. Kato, K. Fushimi and Y. Hasegawa, Angew. Chem., Int. Ed., 2013, 52, 6413.